Dong Qing (Orcid ID: 0000-0003-0877-5401)

Wang Weiguang (Orcid ID: 0000-0003-4984-2498)

Xing Wanqiu (Orcid ID: 0000-0002-1714-1809)

Heterogeneous response of global precipitation concentration to global warming

Qing Dong[a,b], Weiguang Wang[a,b]*, Kenneth E. Kunkel[c], Quanxi Shao[d], Wanqiu Xing[a,b], Jia Wei[a,b]

a. *State Key Laboratory of Hydrology-Water Resources and Hydraulic Engineering, Hohai University, Nanjing 210098, China*

b. *College of Hydrology and Water Resources, Hohai University, Nanjing 210098, China*

c. *North Carolina Institute for Climate Studies, North Carolina State University, Asheville, NC, USA*

d. *CSIRO Data 61, Private Bag 5, Wembley, Western Australia 6913, Australia*

*Corresponding author:

This is the author manuscript accepted for publication and has undergone full peer review but has not been through the copyediting, typesetting, pagination and proofreading process, which may lead to differences between this version and the Version of Record. Please cite this article as doi: 10.1002/joc.6851

Dr. Weiguang Wang

State Key Laboratory of Hydrology-Water Resources and Hydraulic Engineering

Hohai University, Nanjing 210098, China

Tel: +86-25-83786786

Fax: +86-25-83786606

Email: wangweiguang2016@126.com

Abstract

This study investigated the change in precipitation concentration due to global warming based on the output of one experiment (a scenario of 1% CO_2 increase per year) from 12 general circulation models provided by the Coupled Model Intercomparison Project Phase 5 (CMIP5). Two different indices were used to describe precipitation concentration: (1) concentration index (CI), which measures the evenness of total precipitation on wet days, and (2) precipitation concentration degree (PCD), which measures the evenness of the annual precipitation distributions over time. We found that widespread increases in CI were distributed over all land areas except for some arid areas, indicating a less uniform distribution of precipitation on wet days in a warming climate caused by CO_2 increasing. We also found that the spatial patterns of changes in PCD are complex, with large regional differences. All of the results suggest a global-scale readjustment of precipitation distribution in magnitude and timing. This kind of readjustment may have significant impacts on climatic and hydrological events and thus cause severe ecological and environmental damage.

Keywords: climate change; precipitation concentration; increased CO_2; climatological regions.

1. Introduction

Large increases in surface temperature, unprecedented in recent human history, have been detected over the past few decades (IPCC, 2013). Besides the apparent increase in global temperature, the hydrological cycle has also changed (Allen and Ingram, 2002; Huntington, 2006; Wu et al., 2013; Wang et al., 2013a). A "rich get richer" mechanism is hypothesized for the changes in the hydrological cycle and is indeed found in observations and model simulations (Held and Soden, 2006; Chou et al., 2009; John et al., 2009; Allan et al., 2010; Trenberth, 2011). While some changes in precipitation do not universally follow this pattern, the subject remains complicated and disputed (Chadwick et al.,

2013; Greve et al., 2014; Sun et al., 2012). Even though no temporal trend is found in global mean precipitation, the temporal and spatial distributions of precipitation have changed (Trenberth, 2011; Sun et al., 2012). An inconsistent regional change in global land precipitation was detected, and the difference between dry and wet regions expanded (Held and Soden, 2006; Allan et al., 2010; Li et al., 2016). The observations, (Trenberth et al., 2003; Groisman et al., 2005; Goswami et al., 2006; Fischer and Knutti, 2015) in agreement with climate models (Wehner, 2004; O'Gorman and Schneider, 2009; Collins et al., 2013; Fischer et al., 2013; Sillmann et al., 2013; Toreti et al., 2013; Donat et al., 2016), show an increase in precipitation extremes with a warming climate and the intensity of extreme precipitation will increase at a faster rate than average precipitation (IPCC, 2013). Moreover, significant changes in wet-day frequencies and consecutive dry days have been identified (Donat et al., 2013; Pal et al., 2013; Rajah et al., 2014). Differences in seasonal precipitation have also become more pronounced over the past three decades, characterized by an increased annual range of precipitation between wet and dry seasons (Chou et al., 2013; Dwyer et al., 2014). Feng et al. (2013) found that the inter-annual variability of seasonality increased over many parts of the dry tropics. Changes in the spatio-temporal distribution of precipitation are responsible for extreme climatic and weather events and lead to potentially disastrous impacts on society, the environment, and ecology (Trenberth et al., 2003; Lenderink and Meijgaard, 2008; Wang et al., 2013b; She et al., 2015).

The detection of anthropogenic influence on changes in climate variables is immensely important for adaptation planning and developing mitigation strategies to address climate change (Min et al., 2011; Fischer and Knutti, 2015; Sarojini et al., 2016; Wang et al., 2017). The rising concentration of atmospheric CO_2 affects the hydrological cycle by increasing the global mean temperature and altering the atmospheric water vapor content (Manabe and Wetherald, 1975; Trenberth, 1999; Bony et al., 2013). Previous studies have attempted to investigate how precipitation

responds to changes in greenhouse gas (GHG) emissions, specifically CO_2 emissions (e.g., Bony et al., 2013; Lau et al., 2013; Pendergrass and Hartmann, 2014; Zhang et al., 2017; Samset et al., 2018; Bal et al., 2019; Sillmann et al., 2019). Precipitation is projected to increase over many parts of the globe in a 4xCO2 world (Bal et al., 2019). Lau et al. (2013) indicated that the frequency of extreme precipitation increased at the expense of a decrease in moderate and light events under the prescribed 1% CO_2 increase; meanwhile, the length of dry periods also increased. Pendergrass and Hartmann (2014) found an increase in rain amounts at all rain rates and a substantial increase in rain at the highest rain rates. Zhang et al. (2017) found that the odds of occurrence of precipitation extremes increased more on a sub-daily scale than on a daily scale due to increased CO_2. Precipitation concentration, representing the extent to which precipitation is concentrated into few events and concentrated in time (seasonally), has proven to be effective for identifying extreme precipitation and describing the heterogeneous distribution of precipitation (Zheng et al., 2017; Caloiero et al., 2019; Sarricolea et al., 2019). High precipitation concentration is responsible for extreme climatic and weather events such as floods and droughts (Li et al., 2011; Wang et al., 2013b). Moreover, precipitation concentration may influence the environment through soil erosion and landslides (Wang et al., 2013b; Caloiero et al., 2019). Also, a change in the timing of precipitation alters the timing of freshwater availability, which is important for water resource management (Tan et al., 2020). Although some attention has been paid to the topic of how extreme precipitation and precipitation intensity change under global CO_2 warming, how precipitation concentration will change in a warming world is still unclear. The summary statistics/characteristics of precipitation in terms of evenness in different amounts and over different times of year are complementary to other evaluation indices such as annual precipitation amount or precipitation intensity and can provide new information about precipitation (Monjo and Martin-Vide, 2016; Serrano-Notivoli et al., 2018).

The central purpose of this article is to understand how precipitation distribution might change from the perspective of precipitation concentration in a warming climate, in response to increased CO_2 emissions. The output of experiments from the Coupled Model Intercomparison Project Phase 5 (CMIP5) provide a resource for assessing the response of climate variables to increased CO_2 emissions (Taylor et al., 2012). This set of data has been used to investigate the changes in precipitation due to increasing CO_2 emissions (e.g., Lau et al., 2013; Pendergrass and Hartmann, 2014; Zhang et al., 2017). This paper uses two different indices to describe different aspects of precipitation concentration: concentration index (CI) and precipitation concentration degree (PCD). CI, proposed by Martin-Vide (2004), measures how the total precipitation is distributed on wet days (i.e., the irregular distribution of total precipitation). Higher CI represents higher percentages of total precipitation over a few rainy days (Martin-Vide, 2004). CI can be used to evaluate the contribution of the heaviest precipitation events to the total amount. We use another index, PCD, to reflect the annual precipitation distribution. PCD, proposed by Zhang and Qian (2003), reflects the degree to which annual total precipitation is distributed over all months of the year (i.e., the temporal distribution of precipitation during the year). Based on the daily precipitation data from the CMIP5 simulations, a response of precipitation concentration to changes in atmospheric CO_2 at global and land scales and in different climatological zones are detected.

2. Materials and Methods

The outputs of 12 CMIP5 models based on a 140-year experiment were selected. Detailed information about the 12 general circulation models (GCMs) is listed in Table 1. The experiment, 1pctCO2, is initialized from the preindustrial control, and the CO_2 concentration is prescribed to increase at 1% per year from the preindustrial value of 285 ppm (Taylor et al., 2012). According to the experiment

design, the CO_2 concentration doubles by year 70 and quadruples by the end of the model run (Taylor et al., 2012). Blocks of 27 years' duration, identical to Lau et al. (2013), were analyzed. The first 27 years of the simulation is defined as the control period. Then, the differences between the mid 27 years (71st–97th)/the last 27 years (114th–140th) and the control period are defined as the response to a doubling/tripling of CO_2 concentrations (DCO2/TCO2). Since the outputs of the CMIP5 models have different spatial resolutions, all of the daily precipitation data were interpolated to a finer resolution (1° × 1°). Moreover, daily precipitation amounts of more than 0.1 mm were used only to avoid the overestimated drizzle in the GCM simulations.

CI is based on the Gini index. Widely used in the field of economics to estimate income inequality, the Gini index was recently introduced to measure the uniformity of climate variables (Rajah et al., 2014; Konapala et al., 2017). As a robust and nondimensional index, the Gini index is given as (Haughton and Khandker, 2007):

$$\mathrm{GI} = 1 - 2\sum_{i=2}^{N}\left(\frac{y_i + y_{i-1}}{2}\left(x_i - x_{i-1}\right)\right) \tag{1}$$

When an exponential distribution is fitted to substitute the polygonal line, the resulting version of the Gini index is referred to as CI (Martin-Vide, 2004). The visual explanation of CI is illustrated in Figure 1(a). The area under the curve is estimated by the integral of the exponential curve between 0 and 100 (Martin-Vide, 2004):

$$\mathrm{A} = \left[\frac{a}{b}e^{bx}\left(x - \frac{1}{b}\right)\right]_0^{100} \tag{2}$$

$$\mathrm{CI} = \left(5000 - \mathrm{A}\right)/\mathrm{A} \tag{3}$$

The coefficients *a* and *b* can be estimated by means of the least squares method. Due to its considerable scientific and practical merits, CI has been employed by numerous researchers to investigate the changing characteristics of regional or global extreme precipitation events (e.g., Martin-Vide, 2004; Wang et al., 2013b; Monjo and Martin-Vide, 2016; Zheng et al., 2017; Caloiero et al., 2019; Sarricolea et al., 2019). As a nondimensional index, the range of CI is from 0 to 1. Higher CI values denote precipitation is more concentrated in a few rainy days, and values closer to 1 have the highest disparity of precipitation. When the total precipitation is distributed evenly across all rainy days, the CI reaches a minimum value of 0. We used the daily precipitation data to calculate CI for each time interval. The limit of 0.1 mm per day was used to distinguish wet and dry days.

Many indices have been proposed to understand the non-uniformity of annual precipitation distribution, such as the widely used seasonality indices SI (Walsh and Lawler, 1981) and S (Feng et al., 2013). However, these indices do not depend on a natural time sequence and cannot reflect temporal variations. This paper uses PCD (Zhang and Qian, 2003) to reflect the temporal distribution of precipitation during the year because PCD can not only reflect the non-uniformity of precipitation over 12 months but can also measure how temporal precipitation is concentrated during the year. Monthly total precipitation can be considered as a vector with both magnitude and direction (Figure 1b). The magnitude is the total precipitation for each month, and the direction is the corresponding angle of each month within the whole year (the direction for a year is designated as a 360° circle) (Zhang and Qian, 2003). The calculation of PCD can be mathematically expressed as:

$$\mathrm{PCD} = \frac{\sqrt{R_x^2 + R_y^2}}{R} \tag{4}$$

$$R_x = \sum r_j \cdot \sin\theta_j \tag{5}$$

$$R_y = \sum r_j \cdot \cos\theta_j \quad (6)$$

$$R = \sum r_j \quad (7)$$

where R is the annual mean total precipitation for each grid data within the study period, r_j represents the mean monthly total precipitation within the year, and θ_j stands for the azimuth of the corresponding month. As a nondimensional index, the range of PCD is from 0 to 1. If annual total precipitation is concentrated into a single month, a maximum PCD is obtained. If annual total precipitation is evenly distributed across the 12 months, the PCD reaches the minimum value of 0.

< Figure 1 here please >

< Table 1 here please >

3. Results

3.1 Changes in precipitation amount and wet days

The percentage changes for each grid cell were calculated independently for the 12 GCMs, and the multi-model ensemble mean (MEM) was computed. Figure 2 displays the geographic distributions for changes in precipitation amount (P) and wet days (WDs) as well as the co-varying changes. More than 73% of the grid cells show positive changes in P. Negative changes are mainly in the Mediterranean region, Central America, the Caribbean region, Southern Australia, and Southern Africa. The zonal mean changes in P at different latitudes show that increases in P are mainly in the 10°N–10°S latitude band and in high latitudes from 45° to the poles. Although the number of grid cells with positive or negative change rates does not vary greatly between the DCO2 and TCO2

scenarios, the magnitude of the change rate in P is larger under the TCO2 scenario than that under DCO2 scenario, indicating that the spatial variations of precipitation are more pronounced with CO_2 warming. The spatial change in WD shows that the decreases in WD are found in half of grid cells and are more pronounced over land regions than over ocean regions. Decreases in WD are mainly distributed in the low and middle latitudes, while increases in WD are distributed mainly over certain desert regions of Africa and Asia and the plateau area of western China.

A decrease in P and increase in WD are found only in a few grid cells, mainly over oceans. An increase in both P and WD, indicating an increase in water resources, occurs in some arid areas, such as large portions of the Arabian Peninsula, the Sahara Desert, and Tibet, which could be a favorable outcome by alleviating aridity in these areas. An increase in both P and WD also occurs at high latitudes and equatorial areas. An increase in P and decrease in WD means precipitation is concentrated into fewer days, which indicates an increased flood threat; some of the affected regions are densely populated, such as areas in East Asia, North America, eastern South Asia, central Europe, and southeastern South America. The areas with decreases in both P and WD, associated with increased aridity, include subtropical regions, such as the Mediterranean, western Asia, Australia, southern Africa, and southern South America and tropical regions, such as southern North America, northern South America, Western Indonesia, northwestern Africa, and northern Brazil. The decrease in WD is also more pronounced under the TCO2 scenario than under the DCO2 scenario, and the decreases are more concentrated over land regions than over ocean regions.

< Figure 2 here please >

3.2 Change in CI

Figure 3 exhibits the spatial pattern of the change rate in CI under the DCO2 and TCO2 scenarios. Stippling illustrates regions where at least 9 of the 12 models (75% of models) agree on the sign of the estimated changes. Reliable and consistent changes are detected under both scenarios. The change in CI is surprisingly uniform, and the change rate is positive over most of the globe. The increase in CI indicates that precipitation is more concentrated in a few events. CI increases are found across all continents with the exception of a few areas in central Australia, northern North Asia, and northern Africa. The change rates of CI are greater under the TCO2 scenario than under the DCO2 scenario. The areas with increases and decreases tend to increase in magnitude, exhibiting a di-pole amplification pattern due to increasing CO_2 emissions. Considering that detection of the change in the distribution of precipitation over land is of high importance, we separately analyzed the change of precipitation concentration at the global scale and the land scale. The Antarctic was not included in the land region statistical analysis because of its special and complicated geographical environment and climatic conditions. The latitudinal distributions of zonal mean CI changes indicate large variability among different GCMs at equatorial and low latitudes (Figure 4). A relatively consistent trend is detected along 30°–60°. The zonal MEM shows an increased trend over all latitudes due to increased CO_2 emissions. When considering land regions only, there are larger differences between all of the GCMs than at the global scale. CanESM2 shows larger increases in CI than other models over tropical land. Moreover, a similar increase at the global scale is displayed over the latitude zonal mean of all land regions due to increased CO_2 emissions.

< Figure 3 here please >

< Figure 4 here please >

3.3 Change in PCD

The mean change rate in PCD over the entire globe under the DCO2 and TCO2 scenarios is shown in Figure 5. Stippling indicates the agreement in the sign of estimated change across at least 9 of the 12 models (75% of models). A strong regional variability in PCD change is detected. The areas with increases in PCD are mainly distributed in the Southern Hemisphere but also include some Northern Hemisphere areas such as southern North America, western Europe, and the areas around the Mediterranean, the Black Sea, and the Caspian. The land areas of increasing and decreasing changes are about equal. The changes of PCD are more pronounced under the TCO2 scenario than under the DCO2 scenario. The number of grid cells with significant increases in PCD is slightly greater under the TCO2 scenario than under the DCO2 scenario. The latitudinal distributions of zonal mean PCD changes are shown in Figure 6. Globally, there is large variability among different GCMs, but most of the models show the same pattern along the different latitudes except at high latitudes. At high latitudes, the simulations of different models sometimes show opposite signs of change. For the Arctic, the model MRI-CGCM3 shows an increase in PCD, while other models show decreases in PCD. The MEM shows a small increase in PCD over 50°S to 50°N, with a relatively high value around 45°S. Similar behavior is found when considering land regions only. Moreover, relatively high changes are displayed for land regions when compared with the global regions.

< Figure 5 here please >

< Figure 6 here please >

3.4 Regional analysis

To provide more insights into the regional changes, 21 climatological regions (Giorgi and Francisco, 2000) were analyzed separately in detail (Table 2). Considerable regional diversity is evident among the 21 land regions (Figure 7). All regions except SAH show a significant increase for CI. Eleven regions show significant decreases in WD. Among them, there are 4 regions (CAM, CNA, SAF, MED) for which the all grid cells have a negative MEM. As for changes in PCD, 3 regions (AMZ, AUS, and SAF) exhibit significant increases, and 2 regions (ALA, NAS) exhibit significant decreases. Considering the CI and WD together, many regions have a significant increase in CI and a significant decrease in WD, mainly in southern North America (WNA, CNA, ENA, and CAM), South America (AMZ, SSA), the Mediterranean area (MED), Australia (AUS), Southeast Asia (SEA), and Central Asia (CAS). Only 1 region (ALA) exhibits a significant increase in both CI and WD. As for changes in CI and PCD, 3 regions located in the Southern Hemisphere (AMZ, AUS, and SAF) display a significant increase in both CI and PCD, and 2 regions distributed in the high latitudes of Northern Hemisphere (NAS and ALA) show significantly increased CI and decreased PCD. The different changes in CI, WD, and PCD can provide meaningful insights into potential regional impacts under global warming. Take the region MED as an example: the increased CI and decreased WD means that the precipitation happens over fewer days and that precipitation is distributed more irregularly, indicating both a potential increased risk of drought or flood events. Moreover, the increase in the PCD indicates that precipitation becomes more concentrated seasonally.

< Table 2 here please >

< Figure 7 here please >

4. Discussion and Conclusions

In this study, we used the outputs from 12 GCMs to examine the effects of CO_2 warming on the characteristics of precipitation concentration. The differences in precipitation concentration under different CO_2 concentrations (the control, DCO2, and TCO2 scenarios) were analyzed. The changes in CI and PCD exhibit different patterns, indicating that the different aspects of precipitation concentration respond differently to CO_2 warming. Multi-model ensemble means exhibit widespread increases in CI over all land areas except for some arid areas, indicating that increased CO_2 can lead to precipitation amounts that are more concentrated over fewer days. By contrast, the changes in PCD, which expresses how precipitation distribution over a year is concentrated, show large regional differences, exhibiting no uniform response to increased CO_2 emissions. Experiments from climate models have indicated that change in atmospheric moisture content is not only explained by natural climate variability but is also caused by human-induced increases in GHG emissions (Santer et al., 2007). GHGs play an important role in precipitation changes with both thermodynamic and dynamic effects (Seager et al., 2010; Zhang and Li, 2016; Pfahl et al., 2017). The increased global surface temperature associated with increased GHGs leads to the increase of atmospheric water content (Min et al., 2011; O'Gorman and Schneider, 2009; O'Gorman, 2015). Increased CO_2 is also inferred to change large-scale circulation (Seager et al., 2010; Lau and Kim, 2015). The wide diversities found in the regional analysis reflect the spatially varying interactions of thermodynamics and dynamics. These diversities among the different regions also reveal the complexity of the climate system and the inhomogeneity of underlying surface conditions (Greve et al., 2014).

For a scenario of 1% CO_2 increase per year, the changes in P over the ocean areas are generally perceived as following the "rich getting richer" pattern, while over land, they show a more complicated pattern. It is worth mentioning that the global warming effects are not all adverse. The increase in P over some arid areas could decrease aridity. As for the changes in WD, widespread

decreases in WD, which increase the risk of drought or flood, are found over some densely populated areas, with potentially large socioeconomic impacts. The change in WD itself can reflect the change in the number of days with precipitation during a given period. Meanwhile, CI can measure the how unevenly the precipitation is distributed within the WD. The changes in CI and WD can provide a summary of the distribution of precipitation amounts for all days. Increasing CI and increasing WD means more precipitation days as well as a less uniform distribution of precipitation amounts; that is, there are greater increases in extreme precipitation days compared to light precipitation days due to increasing CO_2. By contrast, increasing CI and decreasing WD indicates more dry days, reflecting both an increased risk of drought events and more extreme precipitation days, potentially also increase the risk of floods. Previous research indicated that the frequency and amount of extreme precipitation would increaseunder the prescribed 1% CO_2 increase (Lau et al., 2013; Zhang et al., 2017). Lau and Kim (2015) pointed out that the risk of drought would increase in subtropical and tropical land regions due to global warming. Furthermore, although no consistent trend in PCD was shown at a global scale, we found that the PCD in most monsoon regions showed increasing trends, which would increase the risk of flooding. This is generally consistent with the findings of Bal et al. (2019) that the precipitation seasonality index would increase under the 4xCO2 scenario over many parts of the global monsoon regions. Monsoon regions include almost two-thirds of the world's population and play a key role in global freshwater resources distribution (Zhang et al., 2019). Under global warming, the difference between wet and dry seasons would amplify, and the water cycle in the wet season would enhance over monsoon regions (Zhang et al., 2019). Above all, the change in precipitation concentration (the distribution in values and the seasonal timing) will no doubt increase the difficulty for water resources management and flood and drought prevention.

Uncertainties exist in the precipitation simulations using CMIP5 GCMs. The current generation of GCMs use parametrization schemes to represent convection; this may potentially lead to large uncertainties in the response of precipitation concentration to CO_2 forcing (Westra et al., 2014; O'Gorman, 2015; Zhang et al., 2017). Moreover, although there is general agreement on the sign of the changes, the differences among the GCMs may introduce some uncertainty. Furthermore, the change in precipitation distribution is also affected by various factors such as radiation, aerosol concentration, atmosphere–land interactions, and land-use change (Sun et al., 2012; Lau et al., 2013; Zhang and Li, 2016). It is beyond the scope of this study to comprehensively analyze the reasons for the change in precipitation, but it does provide a comprehensive characterization of how precipitation concentration responds to increasing CO_2 emissions. Further study will focus on investigating the physical mechanisms behind the changing structure of daily precipitation.

Acknowledgements

This work was jointly supported by the National Science Foundation of China (51779073, 51979071), the Distinguished Young Fund Project of Jiangsu Natural Science Foundation (BK20180021), the National "Ten Thousand Program" Youth Talent, and the China Scholarship Council (CSC) program for the Grant CSC financial support (No.201806710160) during Qing Dong's visit to North Carolina State University. This work was partially supported by NOAA through the Cooperative Institute for Climate and Satellites–North Carolina under Cooperative Agreement NA14NES432003. We thank the Working Group of the World Climate Research Program on Coupled Modeling, which is responsible for CMIP5. We thank Andrea L. McCarrick for her linguistic assistance for the preparation of this manuscript. The author extends sincere thanks to Editor Dr. Radan Huth, Associate

Editor Dr. Jose Marengo, and anonymous reviewers for their constructive comments, which greatly improved the quality of this paper.

References

Allan, R. P., Soden, B. J., John, V. O., Ingram, W., and Good, P. (2010). Current changes in tropical precipitation. *Environmental Research Letters* 5(2), 025205, DOI: 10.1088/1748-9326/5/2/025205.

Allen, M. R., and Ingram, W. J. (2002). Constraints on future changes in climate and the hydrologic cycle. *Nature* 419, 224–232.

Bal, P. K., Pathak, R., Mishra, S. K., and Sahany, S. (2019). Effects of global warming and solar geoengineering on precipitation seasonality. *Environmental Research Letters* 14, 03401, DOI:10.1088/1748-9326/aafc7d.

Bony, S., Bellon, G., Klocke, D., Sherwood, S., Fermepin, S., and Denvil, S. (2013). Robust direct effect of carbon dioxide on tropical circulation and regional precipitation. *Nature Geoscience* 6(6), 447–451.

Caloiero, T., Coscarelli, R., Gaudio, R. (2019). Spatial and temporal variability of daily precipitation concentration in the Sardinia region (Italy). *International Journal of Climatology* 39, 5006–5021.

Chadwick, R., Boutle, I., and Martin, G. (2013). Spatial Patterns of Precipitation Change in CMIP5: Why the Rich Do Not Get Richer in the Tropics. *Journal of Climate* 26(11), 3803–3822.

Chou, C., Chiang, J. C. H., Lan, C., Chung, C., Liao, Y., and Lee, C. (2013). Increase in the range between wet and dry season precipitation. *Nature Geoscience* 6(4), 263-267.

Chou, C., Neelin, J. D., Chen, C-A. and Tu, J.-Y. (2009). Evaluating the rich-get-richer mechanism in tropical precipitation change under global warming. *Journal of Climate* 22, 1982–2005.

Collins, M., Knutti, R., Arblaster, J., et al (2013). Long-term Climate Change: Projections, Commitments and Irreversibility. In: Climate Change 2013: The Physical Science Basis. Contribution of Working Group I to the Fifth Assessment Report of the Intergovernmental Panel on Climate Change [Stocker et al., (eds)].Cambridge University Press, Cambridge, United Kingdom and New York, NY, USA.

Donat, M. G., Alexander, L. V. Yang, H., et al. (2013). Updated analyses of temperature and precipitation extreme indices since the beginning of the twentieth century: The HadEX2 dataset. *Journal of Geophysical Research-Atmospheres* 118(5), 2098-2118.

Donat, M. G., Lowry, A. L., Alexander, L. V., O Gorman, P. A., and Maher, N. (2016). More extreme precipitation in the world's dry and wet regions. *Nature Climate Change* 6(5), 508–513.

Dwyer, J. G., Biasutti, M., and Sobel, A. H. (2014). The effect of greenhouse gas–induced changes in SST on the annual cycle of zonal mean tropical precipitation. *Journal of Climate* 27, 4544–4565.

Feng, X., Porporato, A. and Rodriguez-Iturbe, I. (2013), Changes in rainfall seasonality in the tropics. Nature Climate Change 3, 811–815, DOI:10.1038/nclimate1907.

Fischer, E. M., Beyerle, U., and Knutti, R. (2013). Robust spatially aggregated projections of climate extremes. *Nature Climate Change* 3, 1033–1038.

Fischer, E. M., and Knutti, R. (2015). Anthropogenic contribution to global occurrence of heavy-precipitation and high-temperature extremes. *Nature Climate Change* 5(6), 560–564.

Giorgi, F., and Francisco, R. (2000). Uncertainties in regional climate change prediction: a regional analysis of ensemble simulations with the HADCM2 coupled AOGCM. *Climate Dynamics* 16(2), 169–182.

Goswami, B.N., Venugopal, V., Sengupta, D., Madhusoodanan, M., Xavier, P.K., 2006. Increasing trend of extreme rain events over India in a warming environment. *Science* 314 (5804), 1442–1445.

Greve, P., Orlowsky, B., Mueller, B., Sheffield, J., Reichstein, M., and Seneviratne, S. I. (2014). Global assessment of trends in wetting and drying over land. *Nature Geoscience* 7(10), 716–721.

Groisman, P. Y., Knight, R. W., Easterling, D. R., Karl, T. R., Hergel, G. C., and Razuvaev, V. N. (2005). Trends in intense precipitation in the climate record. *Journal of Climate* 18(9), 1326–1350.

Haughton J, Khandker SR. 2007. Inequality measures. In Handbook on Poverty and Inequality, Haughton J, Khandker SR (eds). The World Bank: Washington, D.C.

Held, I. M., and Soden, B. J. (2006). Robust responses of the hydrological cycle to global warming. *Journal of Climate* 19(21), 5686–5699.

Huntington, T. G. (2006). Evidence for intensification of the global water cycle: review and synthesis. *Journal of Hydrology* 319(1), 83–95.

Intergovernmental Panel on Climate Change (IPCC) (2013). *Climate Change 2013: The Physical Science Basis. Contribution of Working Group I to the Fifth Assessment Report of the Intergovernmental Panel on Climate Change*, edited by T. F. Stocker et al., Cambridge Univ. Press, Cambridge, U. K., and New York.

John, V. O., Allan, R. P., and Soden, B. J. (2009). How robust are observed and simulated precipitation responses to tropical warming? *Geophysical Research Letters* 36(14), L14702, DOI:10.1029/2009GL038276.

Konapala, G., Mishra, A., and Leung, L. R. (2017). Changes in temporal variability of precipitation over land due to anthropogenic forcings. *Environmental Research Letters* 12(2), 24009, DOI:10.1088/1748-9326/aa568a.

Lau, W. K. M., and Kim, K. (2015). Robust Hadley Circulation changes and increasing global dryness due to CO_2 warming from CMIP5 model projections. *Proceedings of the National Academy of Sciences of the United States of America* 112(12), 3630–3635.

Lau, W. K. M., Wu, H. T., and Kim, K. M. (2013). A canonical response of precipitation characteristics to global warming from CMIP5 models. *Geophysical Research Letters* 40(12), 3163–3169.

Lenderink, G., and Van Meijgaard, E. (2008). Increase in hourly precipitation extremes beyond expectations from temperature changes. *Nature Geoscience* 1(8), 511–514.

Li, B., Chen, Y., Chen, Z., Xiong, H., Lian, L. (2016). Why does precipitation in northwest China show a significant increasing trend from 1960 to 2010? *Atmospheric Research* 167:275–284.

Li, X., Jiang, F., Li, L., and Wang, G. (2011). Spatial and temporal variability of precipitation concentration index, concentration degree and concentration period in Xinjiang, China. *International Journal of Climatology* 31(11), 1679–1693.

Manabe, S., and Wetherald, R. T. (1975). The effects of doubling the CO_2 concentration on the climate of a general circulation model. *Journal of the Atmosphere Sciences* 32, 3–15.

Martin-Vide, J. (2004). Spatial distribution of a daily precipitation concentration index in peninsular Spain. *International Journal of Climatology* 24(8), 959–971.

Min, S., Zhang, X., Zwiers, F. W., and Hegerl, G. C. (2011). Human contribution to more-intense precipitation extremes. *Nature* 470, 378–381.

Monjo, R., and Martin-Vide, J. (2016). Daily precipitation concentration around the world according to several indices. *International Journal of Climatology* 36(11), 3828–3838.

O'Gorman, P. A. (2015). Precipitation Extremes Under Climate Change. *Current Climate Change Reports* 1, 49–59.

O'Gorman, P. A., and Schneider, T. (2009). The physical basis for increases in precipitation extremes in simulations of 21st-century climate change. *Proceedings of the National Academy of Sciences of the United States of America*, 106(35), 14773–14777.

Pal, I., Anderson, B. T., Salvucci, G. D., and Gianotti, D. J. (2013). Shifting seasonality and increasing frequency of precipitation in wet and dry seasons across the U.S. *Geophysical Research Letters* 40, 4030–4035.

Pendergrass, A. G., and Hartmann, D. L. (2014). Changes in the distribution of rain frequency and intensity in response to global warming. *Journal of Climate* 27(22), 8372–8383.

Pfahl, S., O'Gorman, P. A. and Fischer, E. M. (2017). Understanding the regional pattern of projected future changes in extreme precipitation, *Nature Climate Change* 7(6), 423-+, DOI: 10.1038/nclimate3287.

Rajah, K., O'Leary, T., Turner, A., Petrakis, G., Leonard, M., and Westra, S. (2014). Changes to the temporal distribution of daily precipitation. *Geophysical Research Letters* 41(24), 8887–8894.

Samset, B. H., Myhre, G. Forster, P. M., et al (2018). Weak hydrological sensitivity to temperature change over land, independent of climate forcing, *npj Climate and Atmospheric Science* 1(1), 3, DOI: 10.1038/s41612-017-0005-5.

Santer, B. D., Mears, C., Wentz, F. J., Taylor, K. E., and Wehner, M. F. (2007). Identification of human-induced changes in atmospheric moisture content. *Proceedings of the National Academy of Sciences* 104(39), 15248–15253.

Sarojini, B. B., Stott, P. A., and Black, E. (2016). Detection and attribution of human influence on regional precipitation. *Nature Climate Change* 6(7), 669–675.

Sarricolea, P., Meseguer-Ruiz, Ó., Serrano-Notivoli, R., Soto, M. V., Martin-Vide, J. (2019). Trends of daily precipitation concentration in Central-Southern Chile. *Atmospheric Research* 215, 85–98.

Seager, R., Naik, N., and Vecchi, G. A. (2010). Thermodynamic and dynamic mechanisms for large-scale changes in the hydrological cycle in response to global warming. *Journal of Climate* 23(17), 4651–4668.

Serrano-Notivoli, R., Martín-Vide, J., Saz, M.A., Longares, L.A., Beguería, S., Sarricolea, P. and De Luis, M. (2018). Spatio-temporal variability of daily precipitation concentration in Spain based on a high-resolution gridded data set. *International Journal of Climatology* 38(S1), 518–530.

She, D., Shao, Q., Xia, J., Taylor, J. A., Zhang, Y., Zhang, L., Zhang, X., and Zou, L. (2015). Investigating the variation and non-stationarity in precipitation extremes based on the concept of event-based extreme precipitation. *Journal of Hydrology* 530, 785–798.

Sillmann, J., Kharin, V. V., Zwiers, F. W., Zhang, X., and Bronaugh, D. (2013). Climate extremes indices in the CMIP5 multimodel ensemble: Part 2. Future climate projections. *Journal of Geophysical Research: Atmospheres* 118(6), 2473–2493.

Sillmann, J., Stjern, C. W., Myhre, G., et al. (2019). Extreme wet and dry conditions affected differently by greenhouse gases and aerosols, *npj Climate and Atmospheric Science* 2, 7, DOI: 10.1038/s41612-019-0079-3.

Sun, F., Roderick, M. L., and Farquhar, G. D. (2012). Changes in the variability of global land precipitation. *Geophysical Research Letters* 39(19), L19402, DOI: 10.1029/2012GL053369.

Tan, X., Wu, Y., Liu, B., and Chen, S. (2020). Inconsistent changes in global precipitation seasonality in seven precipitation datasets. *Climate Dynamics* 54(5-6), 3091–3108.

Taylor, K. E., Stouffer, R. J., and Meehl, G. A. (2012). An Overview of CMIP5 and the Experiment Design. *Bulletin of the American Meteorological Society* 93(4), 485–498.

Toreti, A., Naveau, P., Zampieri, M., Schindler, A., Scoccimarro, E., Xoplaki, E., Dijkstra, H. A., Gualdi, S., and Luterbacher, J. (2013). Projections of global changes in precipitation extremes from Coupled Model Intercomparison Project Phase 5 models. *Geophysical Research Letters* 40(18), 4887–4892.

Trenberth, K. E. (1999). Conceptual framework for changes of extremes of the hydrological cycle with climate change. *Climatic Change* 42(1), 327–339.

Trenberth, K. E. (2011). Changes in precipitation with climate change, *Climate Research* 47, 123–138.

Trenberth, K. E., Dai, A., Rasmussen, R. M., and Parsons, D. B. (2003). The Changing Character of Precipitation. *Bulletin of the American Meteorological Society* 84(9), 1205–1217.

Walsh, R. P. D, and Lawler, D. M. (1981). Rainfall seasonality: description, spatial patterns and change through time. *Weather* 36(7), 201–208.

Wang, W., Ding, Y., Shao, Q., Xu, J., Jiao, X., Luo, Y., and Yu, Z. (2017). Bayesian multi-model projection of irrigation requirement and water use efficiency in three typical rice plantation region of China based on CMIP5. *Agricultural and Forest Meteorology* 232, 89–105.

Wang, W., Shao, Q., Yang, T., Peng, S., Xing, W., Sun, F., and Luo, Y. (2013a). Quantitative assessment of the impact of climate variability and human activities on runoff changes: a case study in four catchments of the Haihe River basin, China. *Hydrological Processes* 27, 1158–1174.

Wang, W., Xing, W., Yang, T., Shao, Q., Peng, S., Yu, Z., and Yong, B. (2013b). Characterizing the changing behaviours of precipitation concentration in the Yangtze River Basin, China. *Hydrological Processes* 27(24), 3375–3393.

Wehner, M. F. (2004). Predicted twenty-first-century changes in seasonal extreme precipitation events in the parallel climate model. *Journal of Climate 17*(21), 4281–4290.

Westra, S., Fowler, H. J., Evans, J. P., Alexander, L. V., Berg, P., Johnson, F., Kendon, E. J., Lenderink, G., and Roberts, N. M. (2014). Future changes to the intensity and frequency of short-duration extreme rainfall. *Reviews of Geophysics* 52(3), 522–555.

Wu, P., Christidis, N., and Stott, P. (2013). Anthropogenic impact on Earth's hydrological cycle. *Nature Climate Change* 3(9), 807–810.

Zhang, L., and Li, T. (2016). Relative roles of anthropogenic aerosols and greenhouse gases in land and oceanic monsoon changes during past 156 years in CMIP5 models. *Geophysical Research Letters* 43(10), 5295–5301.

Zhang, L., and Qian, Y. (2003). Annual distribution features of precipitation in china and their interannual variations. *Journal of Meteorological Research* 17(2), 146–163.

Zhang, W., Villarini, G., Scoccimarro, E., and Vecchi, G. A. (2017). Stronger influences of increased CO_2 on subdaily precipitation extremes than at the daily scale. *Geophysical Research Letters* 44(14), 7464–7471.

Zhang, W., Zhou, T., Zhang, L., and Zou L. (2019). Future intensification of the water cycle with an enhanced annual cycle over global land monsoon regions. *Journal of Climate* 32(17), 5437–5452.

Zheng, Y., He, Y., and Chen, X. (2017). Spatiotemporal pattern of precipitation concentration and its possible causes in the Pearl River basin, China. *Journal of Cleaner Production* 161, 1020–1031.

Figure Captions

Figure 1. Pictorial explanation of the indices for precipitation distribution: (a) concentration index (CI) and (b) precipitation concentration degree (PCD). The concentration index is calculated as twice the gray shaded area between the 1:1 line and the polygonal line. The polygonal line, as shown by the pink curve, is given by the cumulative value of a variable according to its cumulative frequency. Precipitation concentration degree (PCD) represents the degree that total precipitation is non-uniformly distributed within a year. Monthly total precipitation can be considered as a vector with both magnitude and direction. θ is the angular value (in radians) for each month's precipitation.

Figure 2. Geographic distribution patterns for (a) the co-varying changes in P and WD, (b) the change in P, and (c) the change in WD under the DCO2 (top) and TCO2 (bottom) scenarios. Shown to the right of sub-figures (b) and (c) is the zonal mean change in P and WD, respectively.

Figure 3. Geographic pattern for the distribution of the change rate (%) in CI under the DCO2 (top) and TCO2 (bottom) scenarios. Stippling indicates the agreement in the sign of estimated change across at least 9 of 12 models (75% of models).

Figure 4. The difference of the latitudinal zonal mean change in CI for each of the 12 CMIP5 models under the DCO2 scenario for all regions (land and ocean; top) and land regions only (bottom).

Figure 5. The same as Figure 3, but for PCD.

Figure 6. The same as Figure 4, but for PCD.

Figure 7. The change rate of CI, WD, and PCD with uncertainty ranges for 21 climatological regions under the DCO2 scenario. Black, red, and blue colors represent the change in CI, WD, and PCD, respectively. Best estimate (solid line in the box), mean value (dashed line in the box), and the 25% to 75% range (bottom and top edges of the box) are shown.

Table Captions

Table 1. Details about the CMIP5 models used in this study.

Table 2. Details about the Giorgi climate divisions.

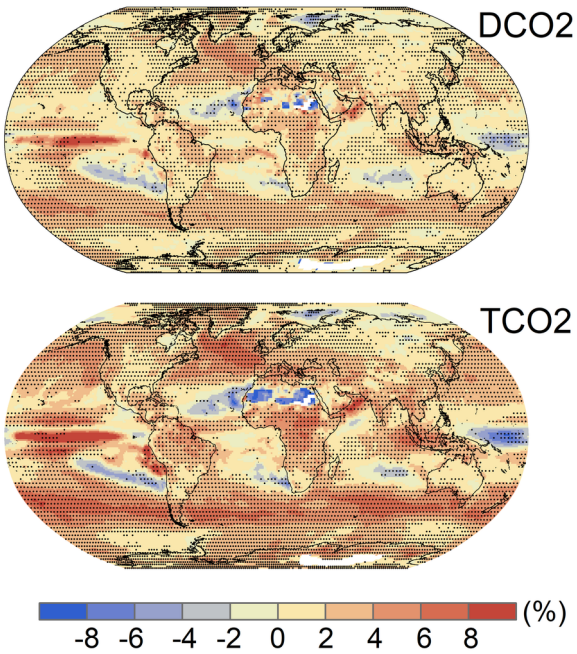

JOC_6851_figure 3.tif

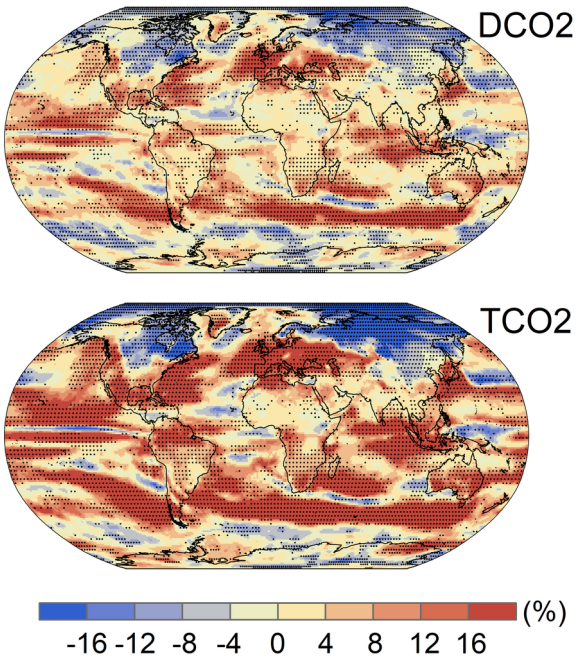

JOC_6851_figure 5.tif

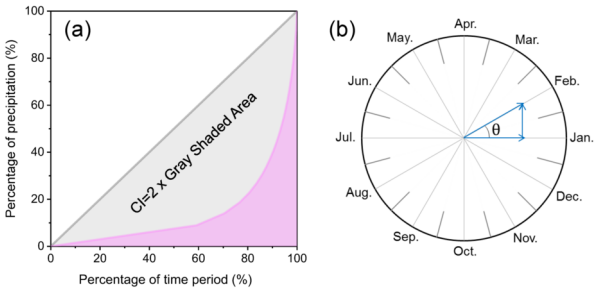

JOC_6851_Figure 1.tif

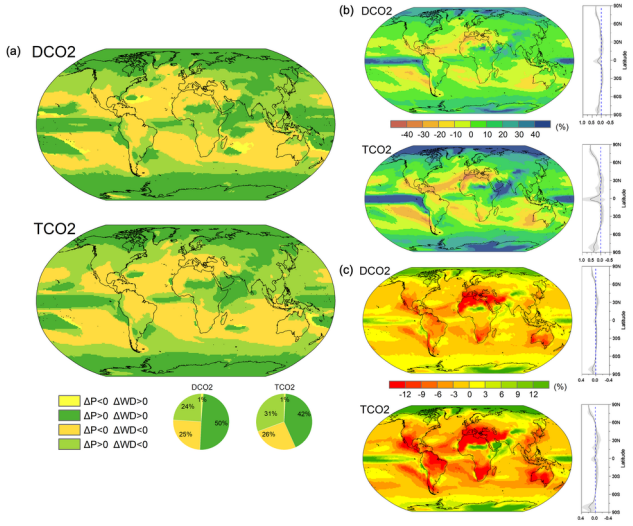

JOC_6851_Figure 2 .tif

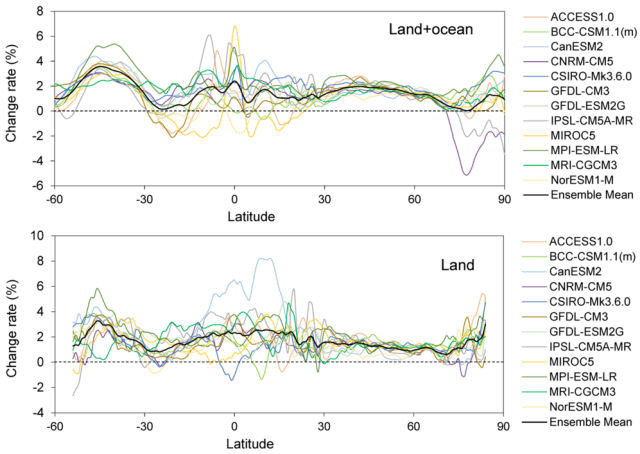

JOC_6851_Figure 4.tif

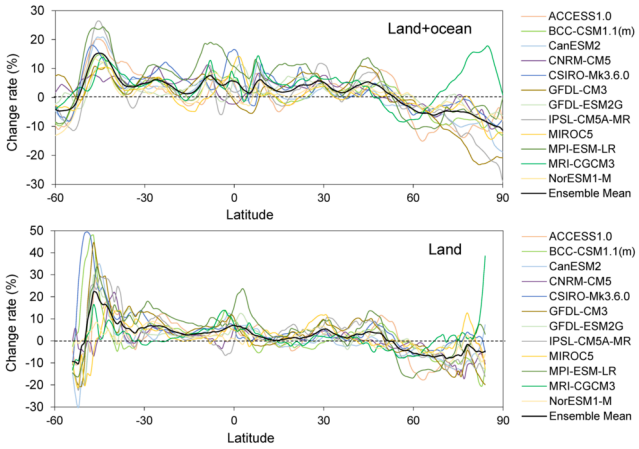

JOC_6851_Figure 6.tif

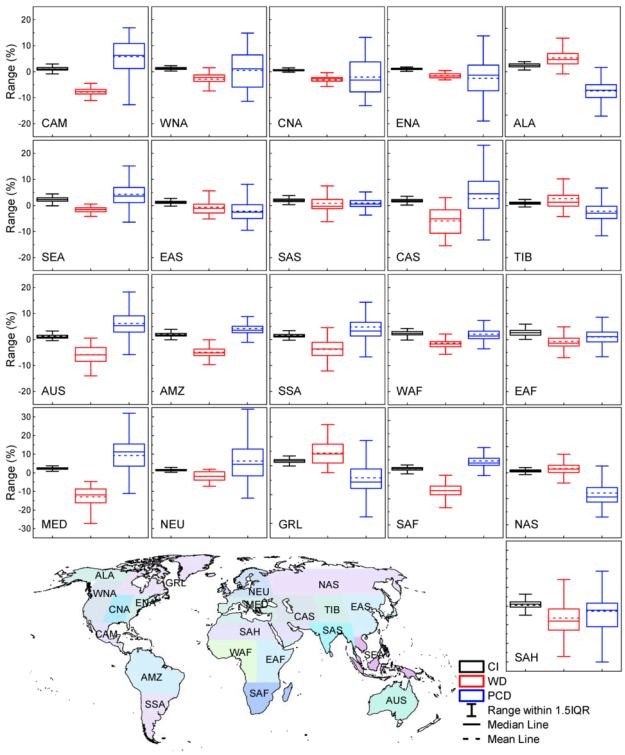

JOC_6851_Figure 7.tif

Heterogeneous response of global precipitation concentration to global warming

Qing Dong, Weiguang Wang*, Kenneth E. Kunkel, Quanxi Shao, Wanqiu Xing, Jia Wei

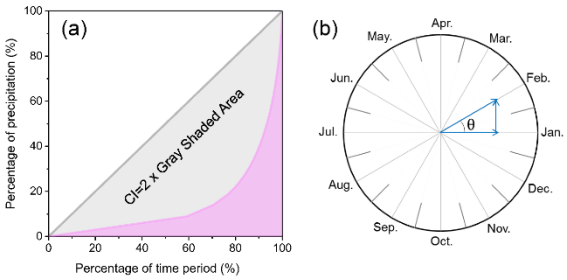

Based on the output of the experiments from the Coupled Model Intercomparison Project Phase 5 (CMIP5), a comprehensive approach from different aspects of precipitation concentration was implemented for assessment of precipitation concentration change due to CO_2 emissions. We found that a global scale readjustment of precipitation distribution in magnitude and timing due to CO_2 increasing. This kind of readjustment would have large impacts on climatic/hydrological events and the environment.

Table 1. Details about CMIP5 model used in this study.

Model name	Modeling center	Resolution
ACCESS1.0	Commonwealth Scientific and Industrial Research Organization/Bureau of Meteorology, Australia	1.25° ×1.88°
BCC-CSM1.1(m)	Beijing Climate Center, China	1.11°×1.13°
CanESM2	Canadian Centre for Climate Modelling and Analysis, Canada	2.79° ×2.81°
CNRM-CM5	Centre National de Recherches Météorologiques, France	~1.4° ×1.4°
CSIRO-Mk3.6.0	Commonwealth Scientific and Industrial Research Organization/Queensland Climate Change Centre of Excellence, Australia	1.86° ×1.88°
GFDL-CM3	Geophysical Fluid Dynamics Laboratory, USA	2.0°×2.5°
GFDL-ESM2G	Geophysical Fluid Dynamics Laboratory, USA	2.0°×2.5°
IPSL-CM5A-MR	Institut Pierre Simon Laplace, France	1.27°×2.5°
MIROC5	Atmosphere and Ocean Research Institute (The University of Tokyo), National Institute for Environmental Studies, and Japan Agency for Marine-Earth Science and Technology, Japan	~1.4° ×1.4°
MPI-ESM-LR	Max Planck Institute for Meteorology, Germany	1.86°×1.88°
MRI-CGCM3	Meteorological Research Institute, Japan	1.11°×1.13°
NorESM1-M	Bjerknes Centre for Climate Research, Norwegian Meteorological Institute, Norway	1.89°×2.5°

Table 2. Details about the Giorgi climate division.

Name	Acronym	Latitude (°)	Longitude (°)
Central America	CAM	10N–30N	116W–83W
Western North America	WNA	30N–60N	130W–103W
Central North America	CNA	30N–50N	103W–85W
Eastern North America	ENA	25N–50N	85W–60W
Alaska	ALA	60N–72N	170W–103W
Southeast Asia	SEA	11S–20N	95E–155E
East Asia	EAS	20N–50N	100E–145E
South Asia	SAS	5N–30N	65E–100E
Central Asia	CAS	30N–50N	40E–75E
Tibet	TIB	30N–50N	75E–100E
Australia	AUS	45S–11S	110E–155E
Amazon Basin	AMZ	20S–12N	82W–34W
Southern South America	SSA	56S–20S	76W–40W
Western Africa	WAF	12S–18N	20W–22E
Eastern Africa	EAF	12S–18N	22E–52E
Mediterranean Basin	MED	30N–48N	10W–40E
Northern Europe	NEU	48N–75N	10W–40E
Greenland	GRL	50N–85N	103W–10W
Southern Africa	SAF	35S–12S	10W–52E
North Asia	NAS	50N–70N	40E–180E
Sahara	SAH	18N–30N	20W–65E